
Automatic Correction of Generative AI Reports using Fact-Checking Model-guided LLMs

Raziuddin Mahmood
RPI

raziuddin.mahmood@gmail.com

Pingkun Yan
RPI

yanp2@rpi.edu

Tanveer Syeda-Mahmood
Stanford University

tanveersyeda1@stanford.edu

Abstract

Automated radiology report generators are being increasingly explored in clinical workflow pilots, particularly for chest X-ray imaging. However, their factual correctness with respect to the description of the findings has often been less than accurate, making their adoption slow and requiring detailed verification by clinical experts. In this paper, we propose an automatic report correction method that uses an image-driven fact-checking model to detect identity and location errors of findings in generative AI reports. Prompts are then generated to correct the sentences by selectively modifying them using a large language model. We show that this method of report correction, on the average, improves the report quality between 17-30% across various SOTA report generators over multi-institutional chest X-ray datasets.

1 Introduction

With the rise in generative AI, a transformative shift is being seen in clinical workflows affecting diagnostic decision support, and personalized treatment planning. Radiology practices, in particular, are piloting automated radiology report generator tools for expediting and streamlining structured report generation[28]. Such reporting tools have progressed the most in chest X-ray radiology thanks to the availability of relatively large datasets such as MIMIC[8] and CheXpert[6] that come with their companion reports for training vision-language generative (VLM) models[1, 4, 11]. However, the results with pilots are revealing a predominance of hallucinations and factual errors which have hampered their adoption in clinical workflows. While these tools continue to be improved, there will still be a need for a fact-checking and correction model that can work with deployed report generators at inference time as a last checkpoint before the information being presented to clinicians.

In this paper, we present a report correction model with a built-in discriminative image-guided fact-checking (FC) model that first detects and localizes the errors in the report. The error analysis along with the original sentences is used to generate a corrective prompt to an LLM which then produces the corrected sentence. We show that this method of report correction improves the report quality of report generators between 17-30% across various SOTA report generators over multi-institutional chest X-ray datasets.

Our paper makes 3 novel contributions. First we generate and contribute to open source, a synthetic dataset called RadCheck consisting of 24 million pairs of image and textual report sentences to represent a large spectrum of correct and incorrect finding descriptions in report generators. Next, we use this dataset to develop and train a novel multi-modal supervised contrastive regression neural network as a fact-checking (FC) model. Finally, the detected errors by the FC model are corrected by a large language model using instructional prompts generated automatically for the incorrect report sentences. Figure 1d illustrates report correction by our method for an automatically generated report in Figure 1 using both the chest X-ray image (Figure 1a) and structured finding descriptions

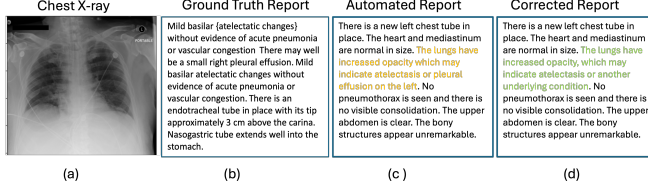


Figure 1: Illustration of report correction. (a) Chest X-ray image. (b) A section of its ground truth radiology report. (c) Automatically generated report by XrayGPT[30]. (d) Corrected report by our method. The sentence with error in finding is colored orange in (c) and corrected sentence is shown in green in (d). Here the erroneous finding of "pleural effusion" is removed while still retaining location information for the remaining finding in the sentence, i.e. atelectasis.

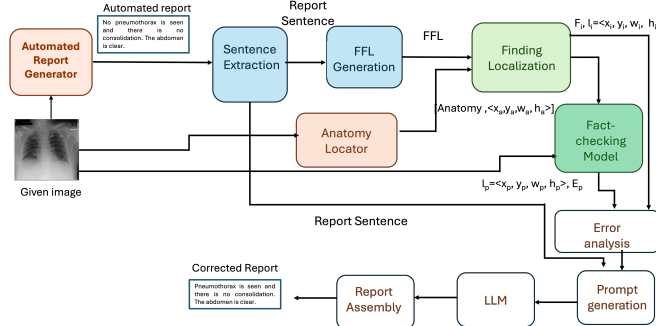


Figure 2: Illustration of the report correction workflow using a fact-checking model-guided LLM.

derived from the automated report in Figure 1c. The result is an improved match to the ground truth report of Figure 1b.

2 Related work

While there is considerable work in chest x-ray radiology report generation literature[1, 2, 3, 13, 19, 24, 25, 28], papers focusing on detecting and correcting errors in radiology report generation have only recently been emerging for inference-time fact-checking[16]. However, the correction approach has been to simply remove the entire sentence. Standard approaches of hallucination reduction through direct policy optimization (DPO)[5, 21, 23, 39] or proximal policy optimization (PPO)[38, 40] are not applicable at clinical inference time. Other inference-time fact-checking methods that consult external knowledge sources cannot be used for patient-specific radiology reports either. [12, 21, 27]. Even powerful LLM-as-a-judge models are not often trained for such domain and patient-specific applications. Thus, to our knowledge, combining fact-checking models with large language models for radiology report correction, has not been previously attempted.

3 Report Correction Method

Our report correction approach addresses the most common types of errors made in radiology reports, namely, false predictions, omissions, and incorrect finding location reporting[26, 36]. The overall report correction process is illustrated in Figure 2. A report produced by an automated report generator for chest X-rays is pre-processed to extract sentences, and findings from sentences. The extracted findings are structured as fine-grained label (FFL) patterns[28], documenting the presence or absence of a finding and any associated anatomical location information. A finding localization algorithm is then used to extract an indicated anatomical image location $l_i = <x_i, y_i, w_i, h_i>$ for the finding from the report. A fact-checking model uses the image I , and the finding pattern F_i to predict an expected location $l_p = <x_p, y_p, w_p, h_p>$ and a veracity label E_p for F_i . The spatial overlap error between the predicted and indicated location along with the veracity indicator E_p is

No	Sentence	FFL
1.	FINDINGS: The heart appears mildly enlarged.	anatomical finding yes enlarged cardiac silhouette heart
2.	Cardiac size is slightly enlarged allowing for limitations of this AP view.	anatomical finding yes enlarged cardiac silhouette heart
3.	Pleural vasculature is not engorged and the patient has moderate pulmonary edema on the right.	anatomical finding no vascular congestion lung anatomical finding yes pulmonary edema lung right

Table 1: Illustration of structured finding extraction using the FFL pattern extraction algorithm[28].

used to generate distinct prompts for different actions in the error analysis module. These are submitted to a large language model (LLM) to perform the sentence correction. The corrected sentences along with valid sentences from the report are combined in order to assemble the overall corrected report.

3.1 Pre-processing

The pre-processing involves parsing of sentences from reports and the extraction of findings. Specifically, we leverage a vocabulary-driven finding pattern (FFL) extraction algorithm that uses a chest X-ray lexicon to find vocabulary terms and their variants within parsed sentences[28]. We chose the FFL extraction algorithm as it could detect the largest number of findings (78 core findings and 101,088 distinct FFL patterns [33]) with over 97% accuracy[28]. Using this algorithm, a finding F_i is described in a structured way as:

$$F_i = T_i|N_i|C_i|A_i|L_i \quad (1)$$

where T_i is the finding type, $N_i = \text{yes}|\text{no}$ indicates a present or absent finding respectively, C_i is the normalized core finding name, A_i is the anatomical location, L_i reflects laterality of the core finding C_i . In this paper, we use F_i to refer to the full FFL pattern as in Equation 1 as well its shortened form $N_i|C_i$ as appropriate. The FFL pattern is a normalized way to describe the finding using standard vocabulary as shown for sentence 1 and 2 in Table 1 for cardiomegaly. Missing anatomical details can also be filled in based on clinical knowledge from a chest X-ray lexicon [34] for the location of a finding as seen in the last sentence in Table 1.

To localize a finding, we first use an anatomical localization algorithm that locates all distinct anatomical regions known to contain chest X-ray findings through bounding boxes [34]. This algorithm detects the largest number of anatomical regions (36 regions) with average localization precision and recall of 0.896 and 0.881 respectively[34] and was used to generated the ChestImaGenome dataset for MIMIC images[8]. The findings are then localized by merging the bounding boxes of the relevant anatomical regions covered by the finding as given by the clinical knowledge in the chest X-ray lexicon[34]. Although this method can over or underestimate the precise boundary of a finding, since locations are only roughly described in radiology reports, this is sufficient for report verification. We rely on clinician-corrected bounding box locations, however, during training the fact-checking model to enable higher precision in localization.

3.2 Generation of synthetic dataset

To train a fact-checking model in a manner agnostic to report generators, instances of report errors made by various automated report generators on large image datasets would be needed as ground truth. Due to the limited availability of clinical expertise for assessing such errors for ground truth generation, as well as to ensure coverage of all current and future automated report generators, we took a different approach to producing the training data for our model. Specifically, we assembled an original dataset of chest X-ray images with their associated clinician-produced radiology reports. We then derived a synthetic dataset of correct and incorrect pairings of images with findings by mixing and matching findings of one image with the another allowing us to create a very large synthetic dataset of over 24 million pairs spanning potentially all major error combinations made by report generators in an efficient and independent manner.

Specifically, let $\langle I, R \rangle$ be a sample set of ground truth image-report pairs in a publicly available dataset D . Let $F = \{F_j\}$ be the total list of possible findings across chest X-ray datasets. Given a real finding f_{ij} at location l_{ij} for a sample image-report pair D_i , we create 3 variants to reflect (a) reversal of polarity (b) relocation of the finding (c) and substitution with appropriate relocation as $FL_{incorrect} = \{\langle \overline{f}_{ij}, f_{ik}, f_{lm} \rangle\}$, where \overline{f}_{ij} is the reversed finding, f_{ik} is finding f_{ij} relocated to a new position $l_k \in L_j$, and f_{lm} is obtained by substituting finding f_j with $f_m \notin F_i$ at location $l_n \in L_m$.

Randomly selecting findings and choosing to vary their locations can create a large variety of combinations. However, to cover both physically plausible (correct/real) as well as impossible combinations (incorrect/fake), we mine the finding statistics in ground truth reports to derive conditional probabilities of co-occurrence of findings. We then adopt a Monte Carlo sampling strategy to introduce randomness in the synthesis process so that those findings that are likely to co-occur frequently do not bias the generation. As a result of this sampling, each data item can be described by the tuple $\langle I, F, \langle x, y, w, h, E \rangle \rangle$ where I is the image, F is an FFL pattern, $\langle x, y, w, h \rangle$ is the bounding box assigned to the finding F and E is a binary label indicating correct/incorrect nature of the findings with $E = 1$ denoting a correct finding.

3.3 Designing the fact-checking model

Our fact-checking model is a multi-modal, multi-label supervised contrastive regression network consisting of a feature learner and a regressor as shown in Figure 3. The feature learner is a contrastive encoder that learns a joint representation of images and short FFL patterns. The regressor learns the association of the combined image-text features with the locations of the findings in the image. Throughout, a supervision label of correct or incorrect association E guides the learning.

Feature learning

A natural choice for a multimodal contrastive encoder is a vision language model such as CLIP[22]. However, unlike CLIP, instead of a single positive image-text pair, we have multiple such pairs corresponding to the findings reported as present or absent in the image. Further, all other pairings are not considered negative as in CLIP since some findings may not even be reported (i.e. are unknown or not important enough to report). Unlike the self-supervision provided by the pairs in CLIP, we have additional supervision coming from the E label indicating the correctness of the finding and location. This results in a non-diagonal similarity matrix for our feature encoder as shown in Figure 3. To train this similarity matrix, we define a multi-label cross-modal supervised contrastive loss function as:

$$\mathcal{L}_{SupC_i} = \frac{-1}{|F_{incorrect}|} \sum_{f_{ij} \in F_{incorrect}} \log \frac{e^{s_{if_{ij}}/\tau}}{\sum_{a_{ik} \in F_{incorrect}} e^{s_{ia_{ik}}/\tau}} \quad (2)$$

where $s_{if_{ij}} = z_i \cdot z_{f_{ij}}$ is the pairwise cosine similarity between image and textual embedding vectors from the correct findings $f_{ij} \in F_{incorrect}$, and $s_{ia_{ik}} = z_i \cdot z_{a_{ik}}$ is with the incorrect findings where $a_{ik} \in F_{incorrect}$. The overall loss is obtained by averaging across all the samples in the batch. Here τ is the temperature parameter. Note that unlike the usual supervised contrastive loss function[10], the summation in the denominator is only over the incorrect findings instead of all negative pairs, thus resulting in a new loss function.

Regression network

The joint embedding space of the feature encoder is not directly suitable for separating the correct from incorrect finding-image associations as the cosine similarity values between their encodings overlap completely. Instead, we found that by forming a high-dimensional feature space by concatenating the contrastively learned image and text embeddings results in better separability between correct and incorrect pairings. The regression classifier, therefore, is a neural network that takes the projected joint embeddings $T_{ijcorrect} = [z_i | z_{f_{ij}}]$ of image I_i paired with correct finding label $f_{ij} \in F_{incorrect}$ or incorrect labels $T_{ijincorrect} = [z_i | z_{a_{ik}}]$ where $a_{ik} \in F_{incorrect}$ and the corresponding supervision label $Y_g = \langle Y_{1g}, Y_{2g} \rangle$ where $Y_{1g} = \langle x, y, w, h \rangle$ is the location and $Y_{2g} = E = 1$ for the real finding and 0 otherwise. Using $Y_p = \langle Y_{1p}, Y_{2p} \rangle$ as the prediction from the network, we can express the regression loss per sample as a combination of an MSE loss

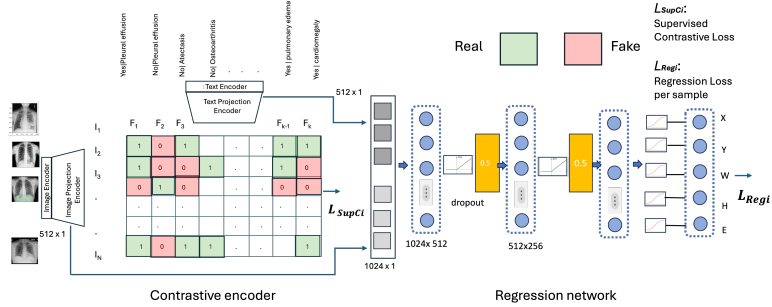


Figure 3: Illustrative of the multimodal supervised contrastive regression network. Here the feature extractor is a supervised contrastive encoder training with a non-diagonal similarity matrix. The classification network is a regressor on both the location and veracity of the label using the combined image and textual input from the finding pattern.

measuring the spatial overlap in location and a binary cross-entropy loss for the correctness of the predicted finding, reflecting the dual attributes being optimized as:

$$\mathcal{L}_{Reg_i} = \underbrace{|Y_{1p} - Y_{1g}|^2}_{\mathcal{L}_{Spatial_i}} - \underbrace{[Y_{2g} \log(Y_{2p}) + (1 - Y_{2g}) \log(1 - Y_{2p})]}_{\mathcal{L}_{Identity_i}} \quad (3)$$

Implementing the FC Model

Bringing these two networks together, the fact-checking model was trained as a single end-to-end learning network as shown in Figure 3. The encoder model was based on a chest X-ray pre-trained CLIP and reused its image and text encoders[24]. The joint embedding projection layers of this model (768x512 for image and 512x512 for text) were, however, fresh-trained using the new supervised contrastive loss mentioned in Equation 2. The regression network (657,413 parameters) consists of two linear layers, two drop out layers followed by a RELU for the intermediate layers and separate sigmoidal functions for producing the output regression vectors as shown in Figure 3. The losses defined in Equations 2 and 3 were applied at the respective heads with the backpropagation for the regression loss going back into the contrastive learning part as well. The total trainable parameters were 151,277,313 parameters making it possible to build this model on an NVIDIA A100 GPU with 40GB of memory. The network was trained for 100 epochs using the AdamW optimizer with a batch size of 32. The cosine annealing learning rate scheduler was used with the maximum learning rate of 1e-5 and 50 steps for warm up.

3.4 Report correction

To correct the reports, the output of the FC model is analyzed. Given an indicated finding F_i extracted from the automated report associated with a given image I at inference time, it can predict a location $l_p = \langle x_p, y_p, w_p, h_p, E_p \rangle$. Using the finding localization algorithm of Section 3.1, we can also derive the finding's indicated location as $l_i = \langle x_i, y_i, w_i, h_i \rangle$. The corrective action rules are formed both using the predicted veracity indicator E_p and the spatial overlap between l_i and l_p measured through IOU as

$$\overline{IOU_{pi}} = 1 - IOU_{pi} = 1 - \frac{|l_p \cap l_i|}{|l_p \cup l_i|} \quad (4)$$

Given the possible values of $l_p, E_p, F_i, \overline{IOU_{pi}}$, there could be a large number of error cases to consider. To simplify the analysis, we quantized these values into ranges. For F_i we consider two major classes of findings, namely, presence findings and absence findings as the location indicators are very different for these. The absence findings are associated with the location coordinates $\langle 0, 0, 0, 0 \rangle$ in both l_i and l_p if predicted correctly. Thus the values of l_p could be categorized into two categories if $l_p \approx 0 = \langle 0, 0, 0, 0 \rangle$ or > 0 . The veracity label E_p is already a binary indicator. Similarly, $\overline{IOU_{pi}}$ can be thresholded by a parameter Γ to indicate a small difference in the spatial

Table 2: Illustration of error analysis using the output of the FC model. The error interpretation and suggested corrective action for a finding F_i mentioned in the sentence S_i are shown in the table.

l_p	E_p	F_p	\overline{IOU}_{pi}	Interpretation	Corrective Action	Prompt
≈ 0	1	Absence	$\leq \Gamma$	Both finding and location are correct.	Do nothing as it is correct.	None
> 0	0	Absence	$> \Gamma$	Finding is present as per FC.	Flip the finding from absence to presence. Leave the location unspecified.	Remove "no $< F_i >$ " and add "yes $< F_i >$ " in the sentence: $< S_i >$
≈ 0	0	Presence	$\leq \Gamma$	FC Model is saying finding is absent	Flip the finding from present to absent. Leave the location unspecified as it is either close or unspecified already.	Remove "yes $< F_i >$ " and add "no $< F_i >$ " in the sentence: $< S_i >$
≈ 0	0	Presence	$> \Gamma$	FC model is saying finding is absent	Flip the finding from present to absent. Remove location hint since the location is far away.	Remove "yes $< F_i >$ ", add "no $< F_i >$ ", and remove location $< A_i >$ from the sentence: $< S_i >$
> 0	1	Presence	$\leq \Gamma$	Both finding and location are correct. Finding is a presence finding	Do nothing as it is correct.	None
> 0	1	Presence	$> \Gamma$	Finding is correct and present but location is wrong	Drop location only. Keep the finding.	Remove location $< A_i >$ from the sentence: $< S_i >$
All other combinations.				Either E_p or l_p is incorrect.	Do Nothing as FC Model itself is incorrect.	None

Table 3: Details of the datasets used in experiments.

Dataset	Patients Train/Val/Test	Images	Findings	Regions	Real/Synth.
RadCheck[14]	44,133/6,274/12,538	243,311	49	922,295	1.616M/27.047M
CIImaGenomeG[34]	288/33/69	461	35	5,477	4,063/23,463
MS-CXR[8]	478/54/114	925	8	2,254	2,247/24,338
ChestXray8[31]	457/51/109	880	8	1,571	1,571/10,137
VinDr-CXR[17]	9,450/1,050/2,250	15,000	23	69,052	47,973/132,632

location ($\overline{IOU}_{pi} \leq \Gamma$) or not. Here we choose $\Gamma = 0.01$ in normalized image coordinates as that was empirically found to be the gap between anatomical regions in chest X-ray regional annotations. With this quantization, we have $2 \times 2 \times 2 \times 2 = 16$ possible combinations to analyze for errors. Of these, the combination ($L_p = 0, E_p = 1, \overline{IOU}_{pi} > \Gamma$) is impossible for an absent finding since its location is not mentioned in reports. Of the 15 combinations, 6 correspond to consistent output from the FC model. These were manually analyzed to arrive at an interpretation and a corrective action, from which 5 unique prompt templates were designed as shown in Column 6 of Table 2. The remaining combinations were potential inconsistency cases in the prediction of the FC model itself. While the FC model performed well across the datasets tested, a potential error in the FC model could potentially worsen the report quality. Fortunately, because we regressed on both location and veracity, we can spot such inconsistencies through these combinations to conservatively disable any corrective action. For example, a combination of ($L_p = 0, E_p = 0, \overline{IOU}_{pi} \leq \Gamma$) for an absent finding F_i is a case where either the location prediction or the veracity indicator is incorrect.

LLM-based sentence correction

Given the FFL patterns and sentences extracted from automated reports, instances of prompts are obtained using the prompt templates indicated in Column 6 Table 2 and given to a large language model to initiate sentence modification and correction. Specifically, we used Llama3.2 as it was freely available and fit within the GPU size of our server. The sentence returned by the LLM are then assembled to form the corrected report. Since duplicate sentences could arise from multiple findings being edited in a given sentence, they are detected and removed. Depending on the order of findings edited, the actual sentences in the corrected report may come in a different order than the automated report, which can also be corrected in a post-processing final step of assembly.

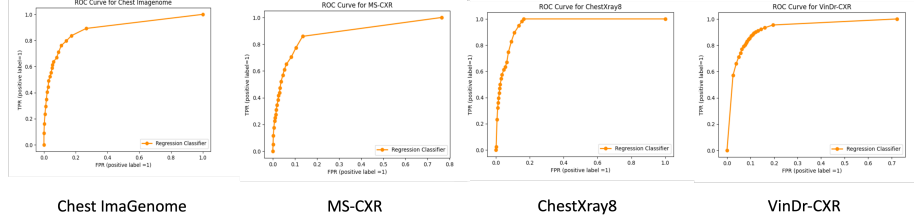


Figure 4: Illustration of FC model accuracy in correct/incorrect finding classification across the test splits of multiple datasets.(a) Chest Imagenome Gold dataset (b) MS-CXR, (c) ChestXray8 from NIH, and (d) VinDr-CXR.

Table 4: Illustration of LLM-based report correction showing the original sentence, the incorrect finding, the actual LLM prompt generated, and the resulting corrected sentence.

Original Sentence	Incorrect finding	LLM Prompt (w/o sentence)	LLM-Corrected Sentence
Left-sided pleural effusion found and the right atelectasis still remains.	yes pleural effusion	Remove "pleural effusion" from sentence:	Right atelectasis still remains.
The chest x ray image shows no focal consolidation, pulmonary edema, pleural effusion or pneumothorax	no pneumothorax	Remove "no pneumothorax" from the sentence:	The chest X-ray image shows no focal consolidation, pulmonary edema, pleural effusion.
The chest x ray image shows no focal consolidation, pulmonary edema, pleural effusion or pneumothorax	no pneumothorax	Remove "no pneumothorax" and add "yes pneumothorax" in the sentence:	The chest X-ray image shows no focal consolidation, pulmonary edema, or pleural effusion, but shows pneumothorax.
There is left pleural effusion and pneumothorax	yes pleural effusion	Remove "left pleural effusion" but keep the "left pneumothorax" in the sentence:	There is left pneumothorax.
The chest x ray image shows no left focal consolidation.	no consolidation	Remove "left" from the sentence:	The chest x ray image shows no focal consolidation.

Table 5: Illustration of FC model evaluation under multiple datasets. The last two rows show comparison with two SOTA methods for fact-checking and phrasal grounding. Here CG stands for ChestImaGenome Gold, C8 is ChestXray-8, MCXR is MS-CXR, and VinDr stands for VindDr-CXR.

Method	Metric	CG	MCXR	C8	VinDr
FC Model	Accuracy	0.92	0.94	0.92	0.90
FC Model	MIOU	0.54	0.53	0.57	0.49
R/F Model	Accuracy	0.84	0.78	0.81	0.83
Maira-2	MIOU	0.39	0.48	0.51	0.42

Table 6: Illustration of the report quality improvement using fact-checking guided LLM using various report quality metrics. Here RadF1 stands for Radgraph F1.

Generator	RadF1		RQ		BLEU		SBERT	
	(A,G)	(C,G)	(A,G)	(C,G)	(A,G)	(C,G)	(A,G)	(C,G)
RGRG[29]	0.52	0.67	0.46	0.52	0.24	0.29	0.33	0.43
XrayGPT[30]	0.39	0.45	0.37	0.48	0.14	0.24	0.26	0.38
GPT4-in	0.43	0.51	0.35	0.47	0.11	0.19	0.09	0.14
R2GenGPT[32]	0.54	0.58	0.37	0.49	0.19	0.27	0.38	0.47
CV2GPT[18]	0.41	0.49	0.38	0.48	0.14	0.24	0.43	0.54
CheXRepair[24]	0.38	0.43	0.36	0.44	0.21	0.28	0.39	0.46
Maira-2[1]	0.58	0.63	0.52	0.59	0.20	0.26	0.43	0.51
Avg.Improv.	13.5%		27%		48.2%		32.5%	

4 Results

We now report our evaluation of the report correction approach using multiple benchmark datasets and report generators.

Datasets used and created

We selected several publicly available multi-institutional datasets of chest X-ray images annotated for findings and their locations as summarized in Table 3. All datasets were clinician validated and vetted for bias and fairness during their IRB approval. For training the fact-checking model, we created a synthetic dataset as described in Section 3.2 starting from the ChestImaGenome Silver dataset[35] which in turn was derived from MIMIC-CXR[9]. The resulting dataset called RadCheck contains over 24 million samples of image pairings with both correct and incorrect finding-location descriptions and is now available in open source on Huggingface[14]. Finally, as other datasets listed in Table 3 already provided findings and locations without ground truth reports, we used the same mixing and matching methodology specified in Section 3.2 to create the correct and incorrect pairings for our evaluations experiments. The testing partitions of the datasets were used for the evaluations, while the training partition of RadCheck was used for training the FC model.

Report generators

We also selected 7 SOTA automated report generators whose Github code was freely available. These included MAIRA-2[1], ChexRepair[24], RGRG[29], XrayGPT[30], R2GenGPT[32], CV2DistillGPT2[18] and our in-house hospital implementation of GPT-4 (GPT4-inhouse). These included automated report generation methods that are based on the latest LLava-style VLM models, with varying capabilities including phrasal ground (RGRG), multi-view and longitudinal information handling (MAIRA-2), and distillation-based models.

Finding error detection performance

We evaluated the accuracy of FC model in finding veracity prediction and localization using the test partitions of the datasets shown in Table 3. The performance was seen to remain stable for different datasets as shown by the ROC curves across datasets in Figure 4. The model consistently yielded an accuracy over 90% for correct/incorrect finding classification, as shown in Table 5. By using 10 fold cross-validation in the generation of the (70-10-20) splits for the datasets, the average accuracy of the test sets lay in the range 0.92 ± 0.12 . In addition, we measured the spatial localization performance through mean IOU measure of spatial overlap between the predicted and ground truth bounding boxes of finding provided in the datasets. This was found to lie in the range 0.49-0.57, indicating that the predicted locations of findings from the fact-checking model have at least 50% overlap with the ground truth finding locations.

Comparison to other methods

With no prior work on fact-checking with phrasal grounding for chest X-ray reports, we compared to the nearest methods that either do phrasal grounding Maira-2[1] or real/fake classification (the R/F Model from [16]). The results are shown in Table 5 with the last two rows recording the relevant numbers for a regressor or classifier respectively showing that the FC Model outperforms both these methods across all the datasets.

Report correction performance

Using an LLM to correct report sentences based on the corrective action templates provided in Table 2 resulted in well-formed sentences with the erroneous portions removed. Table 4 shows examples of report sentences corrected through the LLM in this manner. As can be seen, the resulting sentences are properly formatted language-wise, and reflect the intended corrective action.

To objectively measure the performance improvement across report generators, we ran the report generation tools on the test partitions of all the datasets. We then extracted the findings (FFL patterns) and their anatomical locations as described in Section 3.1. A similar processing was applied to the corrected reports and the ground truth reports when available.

Report quality improvement across metrics

We then recorded the report quality improvement by noting the difference in similarity between automated report (A) to the ground truth report (A,G), versus the similarity between corrected report (C)

Table 7: Illustration of report quality improvement using RQ score across various datasets and report generators. In each case, the corrected report (C) shows higher similarity to the ground truth report (G) than the automated report. Here CG=ChestImaGenome Gold, C8=Chest-Xray8, and VinDr=VinDr-CXR datasets.

Generator	CG		MCXR		C8		VinDr	
	RQ		RQ		RQ		RQ	
	(A,C)	(A,G)	(A,C)	(A,G)	(A,C)	(A,G)	(A,C)	(A,G)
RGRG[29]	0.46	0.52	0.51	0.62	0.38	0.49	0.51	0.63
XrayGPT[30]	0.37	0.48	0.45	0.49	0.35	0.42	0.46	0.54
GPT4-inhouse	0.35	0.47	0.46	0.54	0.41	0.48	0.51	0.58
R2GenGPT[32]	0.37	0.49	0.44	0.54	0.38	0.47	0.51	0.57
CV2DistillGPT2[18]	0.38	0.48	0.39	0.49	0.41	0.47	0.52	0.6
CheXRepair[24]	0.36	0.44	0.45	0.51	0.43	0.49	0.51	0.59
Maira-2[1]	0.52	0.59	0.47	0.58	0.41	0.49	0.50	0.61
Avg. Impv.	13.5%		18.7%		19.14%		16.5%	

and the ground truth report (C,G). The similarity between two reports was measured using several metrics, selecting representative methods from lexical word overlap scores (BLEU[20]), semantic textual matching (SBERT[37]), clinical accuracy F1-score [7], and phrasal-grounded accuracy such as RQ[15]. We used the Chest ImaGenome Gold dataset for this experiment as it had ground truth report with clinician validated findings. The resulting values of these metrics across the report generators for this dataset are shown in Table 6. This table indicates that the report quality improved across all report generators independent of which metric was used for comparison with improvements ranging from 13.5%-48.2% across the metrics and an average around 30.5% improvement seen for this dataset.

Report quality improvement across datasets

Finally, we evaluated the generalization of the report quality improvement performance across multiple datasets and report generators. Since some of the metrics (BLEU, SBERT) needed full ground truth reports which were not available for all datasets, we focused the evaluation using the RQ score as it utilized the finding as well as location information in the provided ground truth across datasets. The resulting performance of the 7 report generators tested across 4 datasets is shown in Table 7. Since RQ score recorded agreement in the finding identity and spatial overlap in the locations of findings, it was able to capture the combined improvement in report quality well across all datasets for all report generators tested, averaging an improvement around 17% across the datasets as shown in that table.

Limitations

Although our work is the first to date to correct radiology reports in this automated way, it does have limitations. Due to limited scope, it does not address severity and measurement errors relating to findings. Secondly, the corrections can be applied to only mentioned findings in reports while missed mentions cannot be added to the report. Next, potential errors in finding extraction and localization could lead to prediction error in the FC model and inconsistencies in error interpretation leading to the selection of incorrect prompts. Finally, the phrasal grounding is currently using bounding boxes which only approximately localize a finding. Full-fledged segmentation of findings may lead to better results. Due to space limitations, we have not reported here the performance of our model in terms of the type of finding errors and their criticality. Finally, the LLM-based report correction can be continually improved with the design of more specific prompts per finding further specializing the templates. Since their output is not guaranteed to be the same in each run, variability could still exist in the reports. These issues will be addressed in future work.

5 Conclusions

In this paper, we have presented a novel method of correction of generative AI reports for chest X-rays by focusing on findings. We developed a fact-checking model covering a large fraction of finding errors and interpreted its output to carve out a set of corrective actions and suitable prompts to result in a higher quality report. Working across data sets and report generators, we have shown an average improvement in report quality ranging from 17-30% across report generators. We hope that such a report correction approach can expedite the adoption of AI reporting models in clinical workflows in future.

References

- [1] Shruthi Bannur, Kenza Bouzid, Daniel C. Castro, Anton Schwaighofer, Anja Thieme, Sam Bond-Taylor, Maximilian Ilse, Fernando Pérez-García, Valentina Salvatelli, Harshita Sharma, Felix Meissen, Mercy Ranjit, Shaury Srivastav, Julia Gong, Noel C. F. Codella, Fabian Falck, Ozan Oktay, Matthew P. Lungren, Maria Teodora Wetscherek, Javier Alvarez-Valle, and Stephanie L. Hyland. Maira-2: Grounded radiology report generation, 2024.
- [2] Mark Endo, Rayan Krishnan, Viswesh Krishna, Andrew Y. Ng, and Pranav Rajpurkar. Retrieval-based chest x-ray report generation using a pre-trained contrastive language-image model. *Proceedings of Machine Learning Research*, 158:209–219, 11 2021.
- [3] Danyang Gao, Ming Kong, Yongrui Zhao, Jing Huang, Zhengxing Huang, Kun Kuang, Fei Wu, and Qiang Zhu. Simulating doctors’ thinking logic for chest x-ray report generation via transformer-based semantic query learning. *Medical Image Analysis*, 91:102982, 1 2024.
- [4] Jiaxian Guo, Sidi Lu, Han Cai, Weinan Zhang, Yong Yu, and Jun Wang. Long text generation via adversarial training with leaked information. In *AAAI-2018*, pages 5141–5148, 2018.
- [5] R. Hardy, E. K. Sung, D. H. Ro, and P. Rajpurkar. Rextrust: A model for fine-grained hallucination detection in ai-generated radiology reports, December 2024. *arxiv:2412.15264*.
- [6] Jeremy Irvin, Pranav Rajpurkar, Michael Ko, Yifan Yu, Silviana Ciurea-Ilcus, Chris Chute, Henrik Marklund, Behzad Haghgoo, Robyn Ball, Katie Shpanskaya, et al. Chexpert: A large chest radiograph dataset with uncertainty labels and expert comparison. In *Thirty-Third AAAI Conference on Artificial Intelligence*, 2019.
- [7] Saahil Jain, Ashwin Agrawal, Adriel Saporta, Steven Q. H. Truong, Du Nguyen Duong, Tan Bui, Pierre J. Chambon, Yuhao Zhang, Matthew P. Lungren, Andrew Y. Ng, Curtis P. Langlotz, and Pranav Rajpurkar. Radgraph: Extracting clinical entities and relations from radiology reports. *CoRR*, abs/2106.14463, 2021.
- [8] A. E. W. Johnson, T. J. Pollard, S. J. Berkowitz, N. R. Greenbaum, M. P. Lungren, C. y. Deng, R. G. Mark, and S. Horng. Mimic-cxr: A large publicly available database of labeled chest radiographs. *arXiv preprint arXiv:1901.07042*, 2019.
- [9] Alistair E W Johnson, Tom J Pollard, Seth J Berkowitz, Nathaniel R Greenbaum, Matthew P Lungren, Chih-ying Deng, Roger G Mark, and Steven Horng. MIMIC-CXR: A large publicly available database of labeled chest radiographs. *arXiv:1901.07042 [cs.CV]*, 2019.
- [10] Prannay Khosla, Piotr Teterwak, Chen Wang, Aaron Sarna, Yonglong Tian, Phillip Isola, Aaron Maschinot, Ce Liu, and Dilip Krishnan. Supervised contrastive learning. *arXiv preprint arXiv:2004.11362*, 2020.
- [11] Jonathan Krause, Justin Johnson, Ranjay Krishna, and Li Fei-Fei. A hierarchical approach for generating descriptive image paragraphs. In *Proceedings of the IEEE Conference on Computer Vision and Pattern Recognition*, pages 317–325, 2017.
- [12] Nieman Journalism Lab. Ai will start fact-checking. we may not like the results.
- [13] Christy Y Li, Xiaodan Liang, Zhitong Hu, and Eric P Xing. Knowledge-driven encode, retrieve, paraphrase for medical image report generation. *arXiv preprint arXiv:1903.10122*, 2019.
- [14] R. Mahmood. Radcheck - a dataset of real/fake chest x-ray radiology report findings and locations. <https://huggingface.co/datasets/razi-mahmood/RadCheck>, 2025. Accessed: 2025-07-28.
- [15] R. Mahmood et al. Evaluating automated radiology report quality through fine-grained phrasal grounding of clinical findings. In *Proc. IEEE Int. Symp. Biomed. Imaging*, pages 1–5, 2025.
- [16] Razi Mahmood, Ge Wang, Mannudeep Kalra, and Pingkun Yan. Fact-checking of ai-generated reports. *Lecture Notes in Computer Science (including subseries Lecture Notes in Artificial Intelligence and Lecture Notes in Bioinformatics)*, 14349 LNCS:214–223, 7 2023.

[17] Ha Q. Nguyen et al. Vindr-cxr: An open dataset of chest x-rays with radiologist’s annotations. *Scientific Data* 2022 9:1, 9:1–7, 7 2022.

[18] Aaron Nicolson, Jason Dowling, and Bevan Koopman. Improving chest X-ray report generation by leveraging warm starting. *Artificial Intelligence in Medicine*, 144:102633, 2023.

[19] Ting Pang, Peigao Li, and Lijie Zhao. A survey on automatic generation of medical imaging reports based on deep learning. *BioMedical Engineering OnLine*, 22:48, 2023.

[20] Kishore Papineni, Salim Roukos, Todd Ward, and Wei-Jing Zhu. Bleu: a method for automatic evaluation of machine translation. In *Proceedings of the 40th Annual Meeting of the Association for Computational Linguistics*, pages 311–318, Philadelphia, Pennsylvania, USA, July 2002. Association for Computational Linguistics.

[21] Kalpdrum Passi and Aanan Shah. Distinguishing fake and real news of twitter data with the help of machine learning techniques. *ACM International Conference Proceeding Series*, pages 1–8, 8 2022.

[22] Alec Radford, Jong Wook Kim, Chris Hallacy, Aditya Ramesh, Gabriel Goh, Sandhini Agarwal, Girish Sastry, Amanda Askell, Pamela Mishkin, Jack Clark, Gretchen Krueger, and Ilya Sutskever. Learning transferable visual models from natural language supervision. *Proceedings of Machine Learning Research*, 139:8748–8763, 2 2021.

[23] Rafael Rafailov, Archit Sharma, Eric Mitchell, Christopher D Manning, Stefano Ermon, and Chelsea Finn. Direct preference optimization: Your language model is secretly a reward model. In *Thirty-seventh Conference on Neural Information Processing Systems*, 2023.

[24] Vignav Ramesh, Nathan A. Chi, and Pranav Rajpurkar. Improving radiology report generation systems by removing hallucinated references to non-existent priors. *Proceedings of Machine Learning Research*, 193:456–473, 9 2022.

[25] Mercy Ranjit, Gopinath Ganapathy, Ranjit Manuel, and Tanuja Ganu. Retrieval augmented chest x-ray report generation using openai gpt models. *Proceedings of Machine Learning Research*, 219:650–666, 5 2023.

[26] V.M. Rao, S. Zhang†, J N. Acosta, S. Adithan, and P. Rajpurkar. Rexerr: Synthesizing clinically meaningful errors in diagnostic radiology reports. In *Pacific Symposium on Bio-Computing Conference*, pages 1–9, 2025.

[27] Abhijit Suprem and Calton Pu. Midas: Multi-integrated domain adaptive supervision for fake news detection. *ArXiv*, abs/2205.09817, 2022.

[28] Tanveer Syeda-Mahmood, Ken C L Wong, Yaniv Gur, Joy T Wu, Ashutosh Jadhav, Satyananda Kashyap, Alexandros Karargyris, Anup Pillai, Arjun Sharma, Ali Bin Syed, Orest Boyko, and Mehdi Moradi. Chest x-ray report generation through fine-grained label learning. In *MICCAI-2020*, 2020.

[29] Tim Tanida, Philip Müller, Georgios Kaassis, and Daniel Rueckert. Interactive and explainable region-guided radiology report generation. In *CVPR*, 2023.

[30] Omkar Thawkar, Abdelrahman Shaker, Sahal Shaji Mullappilly, Hisham Cholakkal, Rao Muhammad Anwer, Salman Khan, Jorma Laaksonen, and Fahad Shahbaz Khan. Xraygpt: Chest radiographs summarization using medical vision-language models. 6 2023.

[31] Xiaosong Wang, Yifan Peng, Le Lu, Zhiyong Lu, Mohammadhadi Bagheri, and Ronald M Summers. Chestx-ray8: Hospital-scale chest x-ray database and benchmarks on weakly-supervised classification and localization of common thorax diseases. 2017.

[32] Zhanyu Wang, Lingqiao Liu, Lei Wang, and Luping Zhou. R2gengpt: Radiology report generation with frozen llms. *Meta-Radiology*, 1:100033, 11 2023.

[33] J. Wu et al. Ai accelerated human-in-the-loop structuring of radiology reports. In *Proc. American Medical Association Annual Symposium (AMIA)*, page 1305–1314, Nov. 2020.

- [34] Joy T. Wu, Nkechinyere N. Agu, Ismini Lourentzou, Arjun Sharma, Joseph A. Paguio, Jasper S. Yao, Edward C. Dee, William Mitchell, Satyananda Kashyap, Andrea Giovannini, Leo A. Celi, and Mehdi Moradi. Chest imangenome dataset for clinical reasoning. 7 2021.
- [35] Joy T. Wu, Nkechinyere N. Agu, Ismini Lourentzou, Arjun Sharma, Joseph A. Paguio, Jasper S. Yao, Edward C. Dee, William Mitchell, Satyananda Kashyap, Andrea Giovannini, Leo A. Celi, and Mehdi Moradi. Chest imangenome dataset for clinical reasoning. *CoRR*, abs/2108.00316, 2021.
- [36] Feiyang Yu, Mark Endo, Rayan Krishnan, Curtis P Langlotz, Vasantha Kumar Venugopal, and Rajpurkar Correspondence. Evaluating progress in automatic chest x-ray radiology report generation. *Patterns*, 4:100802, 2023.
- [37] Tianyi Zhang, Varsha Kishore, Felix Wu, Kilian Q. Weinberger, and Yoav Artzi. Bertscore: Evaluating text generation with BERT. *CoRR*, abs/1904.09675, 2019.
- [38] Rui Zheng, Shihan Dou, Songyang Gao, Wei Shen, Binghai Wang, Yan Liu, Senjie Jin, Qin Liu, Limao Xiong, Lu Chen, Zhiheng Xi, Yuhao Zhou, Nuo Xu, Wenbin Lai, Minghao Zhu, Rongxiang Weng, Wensen Cheng, Cheng Chang, Zhangyue Yin, Yuan Hua, Haoran Huang, Tianxiang Sun, Hang Yan, Tao Gui, Qi Zhang, Xipeng Qiu, and Xuanjing Huang. Secrets of rlhf in large language models part i: Ppo. 2023.
- [39] Yiyang Zhou, Chenhang Cui, Jaehong Yoon, Linjun Zhang, Zhun Deng, Chelsea Finn, Mohit Bansal, and Huaxiu Yao. Analyzing and mitigating object hallucination in large vision-language models. *arXiv preprint arXiv:2310.00754*, 2023.
- [40] Daniel M. Ziegler, Nisan Stiennon, Jeffrey Wu, Tom B. Brown, Alec Radford, Dario Amodei, Paul Christiano, and Geoffrey Irving. Fine-tuning language models from human preferences. *arXiv preprint arXiv:1909.08593*, 2019.